Applied Physics Letters

Launcher of high-order Bessel vortex beam carrying orbital angular momentum by designing anisotropic holographic metasurface

Cite as: Appl. Phys. Lett. **117**, 243503 (2020); https://doi.org/10.1063/5.0031139
Submitted: 29 September 2020 . Accepted: 21 October 2020 . Published Online: 16 December 2020

Xiangshuai Meng, Xiaoming Chen, Lin Yang, Wei Xue, Anxue Zhang, Wei E. I. Sha, and Qiang Cheng

Applied Physics Letters ARTICLE scitation.org/journal/apl

Launcher of high-order Bessel vortex beam carrying orbital angular momentum by designing anisotropic holographic metasurface

Cite as: Appl. Phys. Lett. **117**, 243503 (2020); doi: 10.1063/5.0031139
Submitted: 29 September 2020 · Accepted: 21 October 2020 ·
Published Online: 16 December 2020

Xiangshuai Meng,[1] Xiaoming Chen,[1,2,a)] Lin Yang,[3] Wei Xue,[1] Anxue Zhang,[1] Wei E. I. Sha,[4] and Qiang Cheng[2,5]

AFFILIATIONS

[1]School of Information and Communications Engineering, Xi'an Jiaotong University, Xi'an 710049, China
[2]State Key Laboratory of Millimeter Waves, Southeast University, Nanjing 210096, China
[3]National Key Laboratory of Antennas and Microwave Technology, Xidian University, Xi'an710071, China
[4]Key Laboratory of Micro-Nano Electronic Devices and Smart Systems of Zhejiang Province, College of Information Science and Electronic Engineering, Zhejiang University, Hangzhou 310027, China
[5]School of Electrical Engineering, Southeast University, Nanjing 210096, China

[a)]**Author to whom correspondence should be addressed:** xiaoming.chen@mail.xjtu.edu.cn

ABSTRACT

In this paper, an ultra-low profile anisotropic holographic metasurface is proposed to generate a linearly polarized high-order Bessel vortex beam carrying orbital angular momentum with predesigned topological charge. Based on the leaky-wave theory and optical holographic principle, the anisotropic impedance pattern can be properly mapped by shaping the quasi-periodic metasurface with different meta-atom sizes. Compared with the prevalent spatial wave-modulated metasurface, this surface wave-modulated holographic metasurface effectively transforms a reference wave excited by a feeding source in a single point at the center of the antenna to a leaky high-order Bessel vortex beam without any extra air feeding, which enables a unique characteristic of error-free alignment between the air feeding and designed metasurface. The good agreement between the numerical simulation and the measured result demonstrates that the proposed approach can be employed to launch a linearly polarized high-order Bessel vortex beam with an arbitrary topological mode of interest.

Generally, the Bessel beam can be specially made by solving the Helmholtz homogenous wave equation in the cylindrical coordinate system.[1] Due to the non-diffracting property and self-healing characteristics inherently exhibited by an ideal Bessel beam, it has attracted considerable attention. Considering the beam-forming principle, an ideal Bessel beam can only be generated by a special apparatus with an infinite aperture and unlimited energy. Moreover, the practical launcher could produce a quasi-Bessel beam possessing the non-diffracting feature within a specific propagation distance.[2] Regarding the self-healing characteristics,[3–5] the Bessel beam can preserve its inherent peculiarities of polarization, amplitude, and phase at a distance of several wavelengths away from the encountered obstacle.

On the other hand, the orbital angular momentum (OAM) was first discovered by Allen in 1992.[6] Since then, the OAM has attracted a lot of attention due to its potential in expanding channel capacity and enhancing the spectrum efficiency. In 2007, Thidé introduced the concept of OAM carried by an electromagnetic (EM) vortex wave,[7] which is closely analogous to the high-order Laguerre–Gaussian (LG) beam. Since then, substantial approaches have been developed to generate high-order quasi-LG vortex waves through using circular array antennas,[9] spiral phase plates,[10] spiral parabolic antennas,[8,11] high-order mode exciting antennas,[12] reflected metasurfaces,[13–15] and transmitted metasurfaces.[16–18] Due to the gradually increasing null area of the quasi-LG vortex wave along the propagation direction, there is a great challenge in the reception of OAM signals, especially over long transmission distance. Interestingly, having both the non-diffracting property originated from the zero-order Bessel and spiral phase attributed from the quasi-LG vortex wave, the high-order Bessel beam carrying OAM named as the pseudo-Bessel vortex wave can alleviate the divergence suffered from the conventional quasi-LG vortex wave. Recently, several Bessel vortex wave launchers have been reported. Inspired by the principle of Bessel beamforming in the THz band, a

perfect high-order Bessel beam can be considered as a superposition of plane waves with wave vectors lying on the helical axicon surface,[19] which can be driven by a planar air-fed metasurface at radio frequency.[20–27] Because of the indispensable external feeding source, the above-mentioned metasurface based on space wave modulation usually needs bulky volume, which in turn deteriorates the antenna performance. Afterwards, the radial line slot array (RLSA) antenna was proposed to validate the capability of collimating the conventional diffracting vortex waves.[28,29] However, it has a weak capability to control the radiation direction, limiting its application for OAM multiplexing.[16–18] In addition, it is worth noting that the isotropic impedance surface also has been investigated to radiate the zero-order Bessel beam,[30] while the polarization and wavefront of the leaky wave cannot be modulated by employing the scalar holographic metasurface.

To reduce the launcher profile while achieving powerful control of the beam radiation direction, polarization state, and space phase, a method of manipulating the coupling between electrical currents and radiative EM fields in any spatial direction is highly desirable. Accordingly, this work invents an anisotropic holographic metasurface based on a majority of meta-atoms with topological tensor impedances to generate a high-order Bessel vortex wave carrying OAM. The design process was verified through experiments. Furthermore, characterized by the ultra-low profile, easy integration, and flexible control of the polarization, wavefront, and radiation direction, the anisotropic holographic metasurface is one of the best candidates to enhance the performance of the launcher for the quasi-Bessel wave with arbitrary OAM mode.

The electric field of the n-order Bessel beam obtained by solving the homogenous Helmholtz equation in the cylindrical coordinate system) can be given by

$$E(r,\varphi,z) = E_0 J_n(k_\perp r)\exp(-jn\varphi)\exp(-jk_z z), \tag{1}$$

where $r^2 = x^2 + y^2$ represents the radius of the field distributed on the cross section perpendicular to the propagation axis, φ denotes the azimuthal angle, and $k_\perp$ and k_z are the wave numbers along the transverse section and z axis direction. In addition, the intensity pattern of the field distribution satisfying the nth-order Bessel function of first kind can be generally referred to as the Bessel beam. When $n = 0$, the beam can be described by the zero-order Bessel without OAM mode due to the absence of the helical phase term. While $n \neq 0$, the beam carrying OAM can be named as the high-order Bessel wave accompanied by the spiral phase wavefront of $\exp(-jn\varphi)$. Based on the function integration, the n-order Bessel function can also be written by

$$J_n(k_\perp r) = \frac{1}{2\pi}\int_0^{2\pi} \exp\left[-jk_\perp(x\cos\varphi + y\sin\varphi)\right]d\varphi. \tag{2}$$

Considering both Eqs. (1) and (2), the principle of generating the high-order Bessel vortex beam (equivalent to the superposition of the planar wave propagating around the helical axicon with a cone angle of δ) is schematically shown in Fig. 1. Without loss of generality, the far field radiation expression of the linearly polarized Bessel vortex is given by

$$\mathbf{E}_{rad} = (1,0,0)\exp\left(-j\vec{k}\cdot\vec{r}_{mn} - jn\varphi_{kmn} - j|\vec{k}||\vec{r}_{mn}|\sin\delta\right), \tag{3}$$

where $\vec{k}$ is the wave vector in free space, $\vec{r}_{mn}$ represents the position vector of the mn^{th} element, $|\vec{r}_{mn}|$ is the distance from the mn^{th} element to the central position of the feeding source, δ denotes the spiral axicon angle, and φ_{kmn} means the azimuthal angle on the plane orthogonal to the wave vector $\vec{k}$.

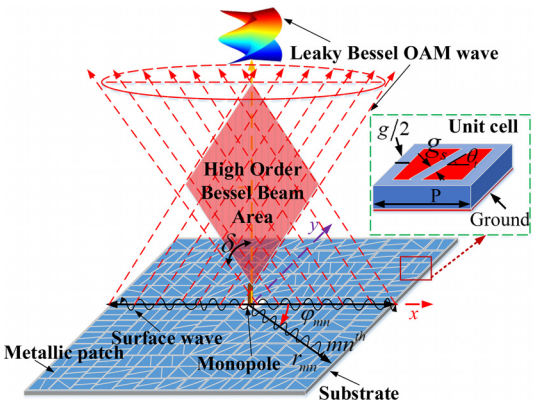

FIG. 1. Schematic mechanism for the metasurface used to generate a high-order Bessel vortex wave carrying OAM mode.

Considering the no-diffracting beam synthesized and characterized in the near-field, the depth of the ideal no-divergence zone should be smaller than the radius of the near-field region, which can be used to limit the minimum spiral axicon angle $\delta_{\min}$. Furthermore, $\vec{k}\cdot\vec{r}_{mn}$ expresses the tangential phase at the metasurface plane related to the radiation direction, $n\varphi_{kmn}$ is considered as the vortex phase with the order number of n, and $|k||\vec{r}_{mn}|\sin\delta$ denotes the phase of the plane waves with wave vectors lying on the spiral cone.

The monopole antenna serving as the feeding point source located at the center of the metasurface can be used to excite the surface wave propagating near the impedance surface, and the surface current can be approximated as the cylindrical wave,

$$\mathbf{J}_{surf} = \frac{(x_{mn}, y_{mn}, 0)}{|\vec{r}_{mn}|}\exp(-jn_e|\vec{k}||\vec{r}_{mn}|), \tag{4}$$

where $(x_{mn}, y_{mn}, 0)$ represents the position coordinate of the mn^{th} element on the array and n_e stands for the effective index seen by the surface currents.

According to the holography theory,[31] the modulated tensor-surface impedance needs to be calculated by the following expression:

$$\begin{aligned}\boldsymbol{Z} &= j\begin{pmatrix} X & 0 \\ 0 & X \end{pmatrix} + j\frac{M}{2}\mathrm{Im}\left(\mathbf{E}_{rad}\otimes\mathbf{J}_{surf}^H - \mathbf{J}_{surf}\otimes\mathbf{E}_{rad}^H\right) \\ &= \begin{pmatrix} jX + j\frac{M}{2}\mathrm{Im}\left(E_xJ_x^H - E_x^HJ_x\right) & j\frac{M}{2}\mathrm{Im}\left(E_xJ_y^H - E_y^HJ_x\right) \\ j\frac{M}{2}\mathrm{Im}\left(E_yJ_x^H - E_x^HJ_y\right) & jX + j\frac{M}{2}\mathrm{Im}\left(E_yJ_y^H - E_y^HJ_y\right) \end{pmatrix},\end{aligned} \tag{5}$$

where the average modulation impedance X and modulation depth M are synthetically determined by the maximum value $Z_{\max}$ and the minimum value $Z_{\min}$ of the effective scalar impedance of the tensor-surface impedance elements used to construct the anisotropic holographic metasurface. Connecting the object wave, Eq. (3), with the reference wave, Eq. (4), to the modulated matrix, Eq. (5), the three deduced components Z_{xx}, Z_{xy}, and Z_{yy} of the tensor-surface impedance with the pointed direction (θ_k, φ_k) arranged on different positions of the anisotropic metasurface can be given by

$$\begin{cases} Z_{xx} = j\left[X + \dfrac{M}{|\vec{r}_{mn}|}x_{mn}\sin(n_e|\vec{k}||\vec{r}_{mn}| - |\vec{k}|x_{mn}\sin\theta_k\cos\varphi_k - |\vec{k}|y_{mn}\sin\theta_k\sin\varphi_k \right. \\ \left. -n\varphi_{kmn} - |\vec{k}||\vec{r}_{mn}|\sin\delta)\right] \\ Z_{xy} = j\dfrac{M}{2|\vec{r}_{mn}|}y_{mn}\sin(n_e|\vec{k}||\vec{r}_{mn}| - |\vec{k}|x_{mn}\sin\theta_k\cos\varphi_k - |\vec{k}|y_{mn}\sin\theta_k\sin\varphi_k \\ \qquad -n\varphi_{kmn} - |\vec{k}||\vec{r}_{mn}|\sin\delta) \\ Z_{yy} = jX. \end{cases} \tag{6}$$

In this design process, the anisotropic holographic metasurface can be considered as a periodic two-dimensional leaky-wave aperture antenna. As schematically shown in Fig. 1, the common sub-wavelength quasi-periodic meta-atom on a grounded dielectric substrate (F4B, $\varepsilon_r = 2.2 + j0.02$) with a period of 3 mm has been developed. Compared with the isotropic unit, the upper-layer metal of this tensor-impedance element is cut with a rectangular slot with a width $g_s = 0.2$ mm passing through their central point. This results in a varied effective scalar impedance along the propagation direction θ_s of the surface wave, when the slotted angle θ_t between the rectangular gap and horizontal axis varies. According to the electromagnetic theory and principle of the guided wave, there exists a hybrid mode of TE and TM surface waves along the modulated tensor-impedance texture. Therefore, an effective scalar-impedance k_z/k_0 equivalent to the tensor-impedance normalized by the free space wave impedance has been explored in depth, which can be given by Ref. 31. Furthermore, in order to obtain the mapping relation between the geometric parameters and the effective scalar-impedance, the CST eigen-mode solution has been employed to calculate the numerical results for the tensor-impedance meta-atom with a variable gap g between adjacent cells and different slot angles θ_t. In our previous works,[32] the gap g determined by the maximum effective scalar-impedance Z_{emax} (that is equivalent to the tensor-impedance normalized by the free space wave impedance) has been explored in depth at the frequency of 20 GHz.

Next, in order to further elaborate the advantages of the high-order Bessel vortex wave over the conventional vortex beam, two anisotropic holographic artificial impedance metasurfaces composed of 101×101 elements with an electric size of $20.2\lambda \times 20.2\lambda$ have been designed to generate a non-diffraction first-order Bessel vortex wave and a conventional first-order diffractive vortex beam at the frequency of 20 GHz, respectively. Moreover, the beam radiation direction is set to $(\theta_k = 0, \varphi_k = 0)$ perpendicular to the planar aperture surface, and the quasi-Bessel vortex beam in our design has a spiral axicon angle $\delta = 2.8°$. The tensor-impedance components distributed on different positions over the metasurface can be calculated, as shown in Fig. 2. Therefore, the gap g needs to be calculated and the slot angle θ_t can be obtained by the normalized scalar-impedance formulation,[33] as shown in Fig. 3.

According to the geometric parameters of the tensor-impedance meta-atoms, full wave simulation has been conducted to calculate the radiation and propagation properties of the EM vortex wave launched by the designed metasurface. Figure 4(a) shows the simulated amplitude distribution of the component of the conventional vortex beam with OAM mode $l = +1$ propagating along the z-axis at the *yoz* plane. It should be noted that the beam divergence range has covered a circular aperture area with a radius of 250 mm at the position of 2 m along the z-axis while compared to the radius of 120 mm at the position of 2 m along the z-axis in Fig. 4(b). Meanwhile, the two separated main beam intensity lines of the hollow-shaped wave have been diffracted to the edge of an observational section plane that is 2 m long along the z-axis and 0.5 m wide along the y-axis. However, in terms of the diffraction-free field originating from the pseudo-Bessel vortex beam, as exhibited in Fig. 4(b), the radius of the circular coverage at the position of 3 m is 120 mm, which is 30 mm larger than that of the annular area at 0.5 m away from the metasurface along the z-axis. After comparing Fig. 4(a) with Fig. 4(b), it can be clearly seen that the divergence feature of the conventional OAM mode is greatly suppressed by the quasi-Bessel vortex beam, resulting in a significantly improved collimation.

Furthermore, to demonstrate the non-diffusion feature from the propagation of the high-order Bessel vortex beam, the amplitude and phase distributions at different positions have been computed.

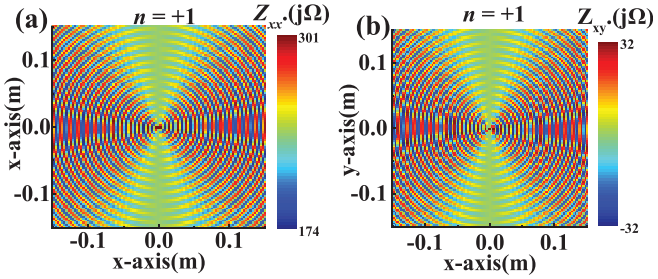

FIG. 2. Tensor impedance component distribution: (a) Z_{xx} and (b) Z_{xy}.

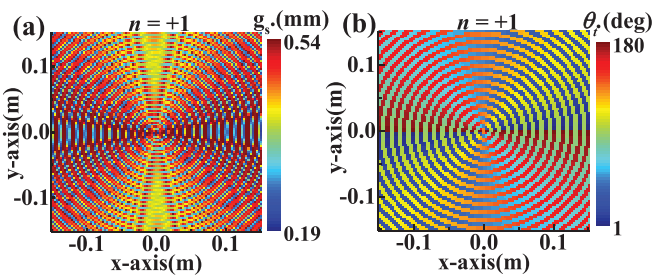

FIG. 3. Geometric parameter distribution for tensor impedance unit: (a) g_s and (b) θ_t.

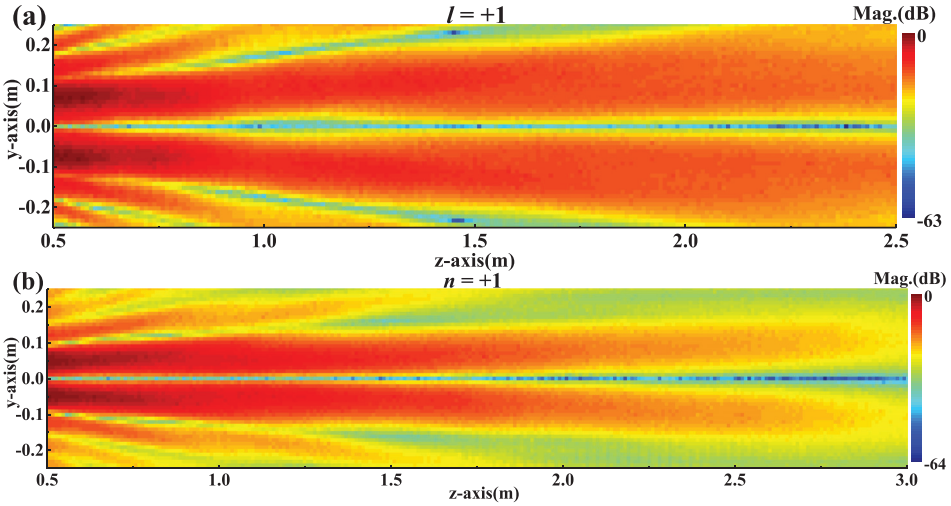

FIG. 4. *E*-field propagation features of the simulated vortex wave with OAM mode of $l = +1$ at the yoz plane along the z-axis direction: amplitude distribution for the (a) divergent vortex wave and (b) high-order Bessel wave.

The coverage radius of the cross section for the conventional vortex beam propagating at the observational plane located 1.0 m(66.6λ), 1.5 m (100λ), 2.0 m (133.3λ) away from the antenna aperture is approximated to 150 mm (10λ), 200 mm (13.3λ), 250 mm (16.6λ), respectively, as shown from Figs. 5(a)–5(c). The hollow energy distribution of the simulated *E*-field along the propagation axis can be clearly seen in Fig. 6. The coverage area grows rapidly with the increasing propagation distance, demonstrating the diffraction characteristics of the conventional vortex beam.

When it comes to the high-order Bessel vortex beam, as shown in Figs. 6(a)–6(c), at different distances of $z = 1.0$ mm (66.6λ), 1.5 m (100λ), and 2.0 m (133.3 λ), the outer radius of the annular non-diffraction *E*-field distributions is close to 100 mm (6.6λ), 110 mm (7.3λ), and 150 mm (10λ), respectively. Compared with the radius increment of 3.3λ for the ring-like magnitude distribution of a conventional vortex beam carrying the $l = +1$ OAM mode, the radius increment in the high-order Bessel vortex beam with the same topological charge has a smaller change of 0.15λ vs the ongoing propagation distance of 33.3λ at the frequency of 20 GHz, at which the diffracting angle has been remarkably reduced. In addition, the chirality of wavefront has no change. In other words, the OAM mode of $l = +1$ remains unchanged during the propagation process, as

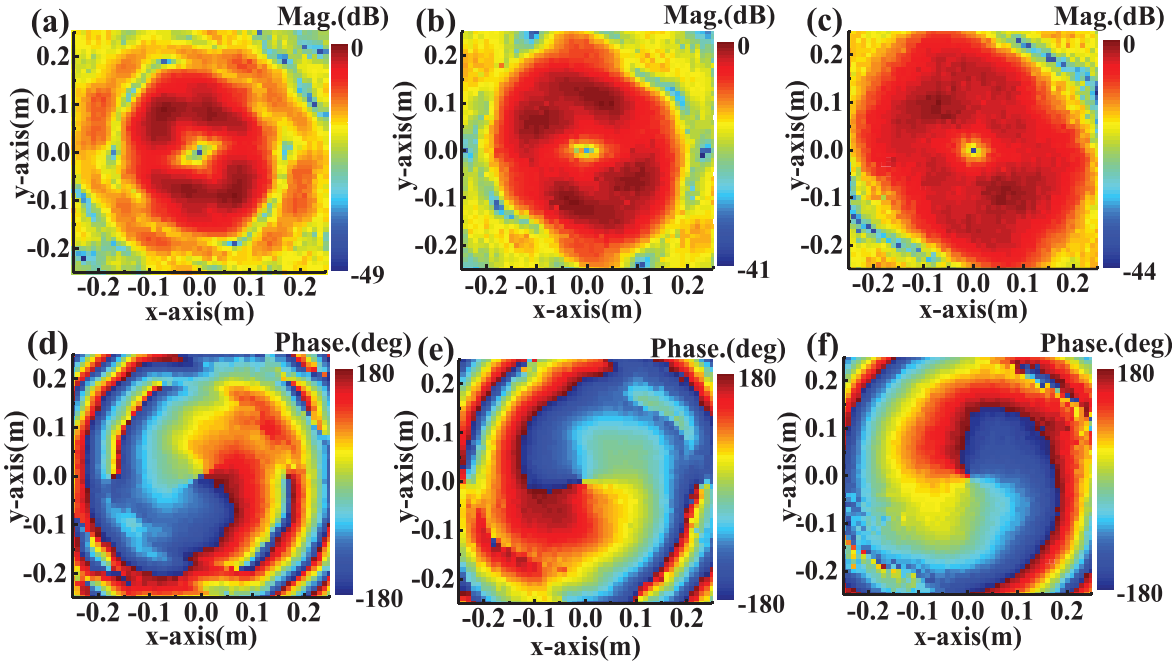

FIG. 5. (a)–(c) Simulated amplitude distributions and (d)–(f) phase patterns on different observational planes located at the cases of 1 m, 1.5 m, and 2 m away from the antenna for the conventional vortex wave at 20 GHz.

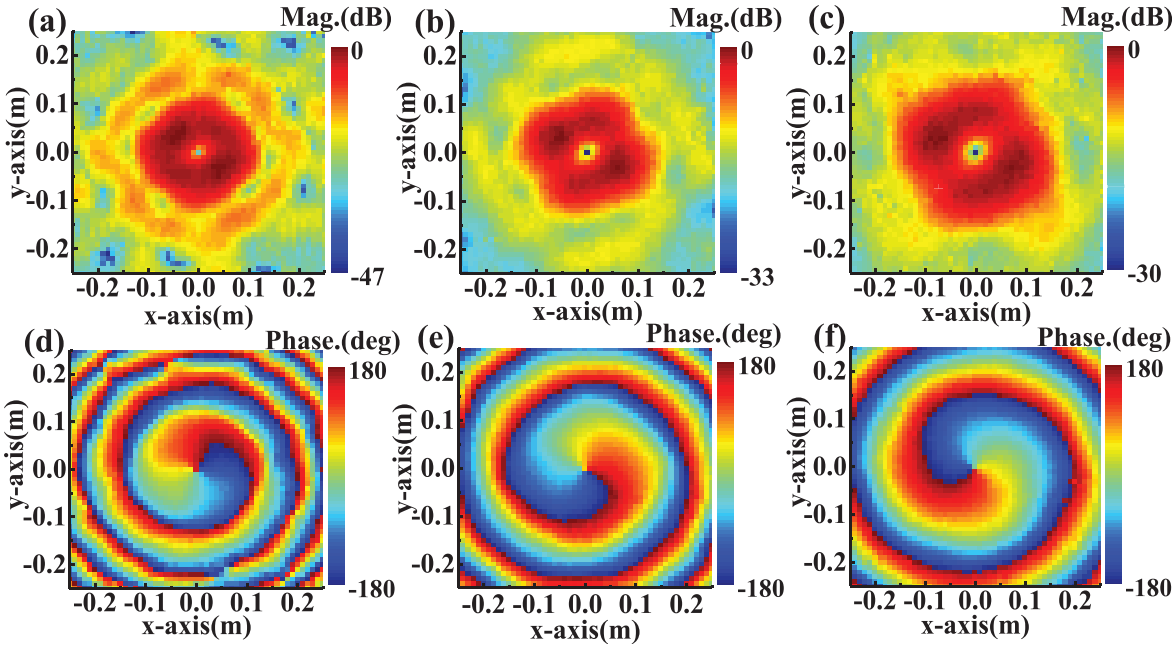

FIG. 6. (a)–(c) Simulated amplitude distributions and (d)–(f) phase patterns on different observational planes located at the cases of 1 m, 1.5 m, and 2 m away from the antenna for the Bessel vortex wave at 20 GHz.

shown from Figs. 6(d)–6(f). Overall, the typical radiation and propagation performance of the vortex beam carrying OAM has not been affected after the cone angle is loaded.

To experimentally evaluate the proposed methodology, a prototype of the anisotropic holographic metasurface for generating a quasi-Bessel vortex beam with OAM mode of $l = +1$ has been designed and manufactured with the printed circuit board (PCB) technology, as shown in Fig. 7. From the S11 shown in Fig. 8(a), the excellent impedance match can be seen from 18 GHz to 22 GHz with an impedance bandwidth of 20%, over which the S11 falls below −15 dB. Note that the reflection coefficient S11 is the ratio of the amplitude of the reflected wave to that of the input wave at a radio frequency (RF) port. The planar near-field scanning approach has been applied to measure the Bessel vortex wave launched by the assembled metasurface antenna in an anechoic chamber, as shown in Fig. 8(b). The normal direction of the prototype under test is arranged to align with that of the open-end rectangle waveguide functioning as the probe operating at 20 GHz. The scanning plane is set to be 60 mm (4λ) away from the probe aperture to receive a 420 mm × 420 mm linear polarized field E_h with a step of 7 mm to fulfill the near-field measurement condition. Based on the near-field measurement data, the far-field radiation pattern can be calculated by the 2D Fast Fourier Transform (FFT) method as depicted in Fig. 9. An obvious zero-depth can be observed in the propagation axis direction with a smaller sidelobe below −10 dB. The slight ripple between the simulated and measured mainlobe is mainly attributed to the manufacturing tolerance and imperfect soldering. Furthermore, the near-field amplitude and phase data at three 500 mm × 500 mm sampling transverse planes located at the distance of 1.0 m (66.6λ), 1.5 m (100λ), and 2.0 m (133.3λ) with respect to the prototype surface are shown in Fig. 10. In particular, the size of the intensity singularity slightly increases with the propagation

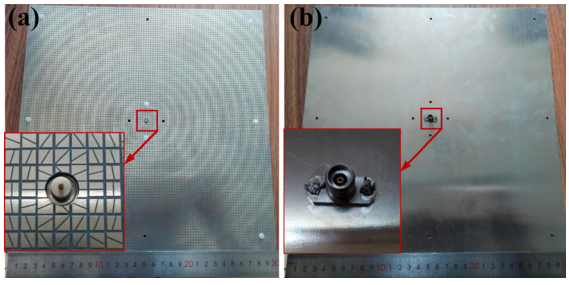

FIG. 7. Configuration of our proposed prototype: (a) top side and (b) back side.

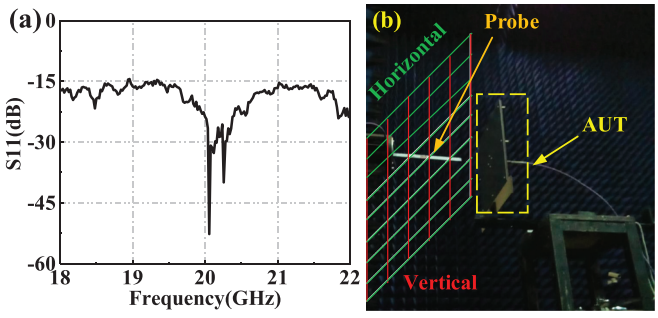

FIG. 8. (a) Measured reflection coefficient of the developed metasurface. (b) Experimental environment for our designed Bessel antenna with the near-field planar scanning method.

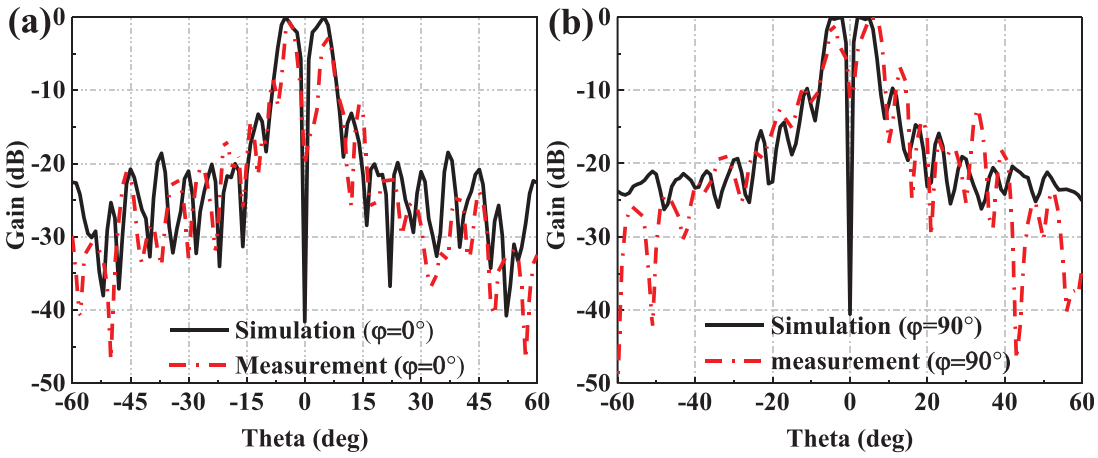

FIG. 9. Simulated and measured 2D far-field radiation pattern for (a) $\varphi = 0^\circ$ and (b) $\varphi = 90^\circ$.

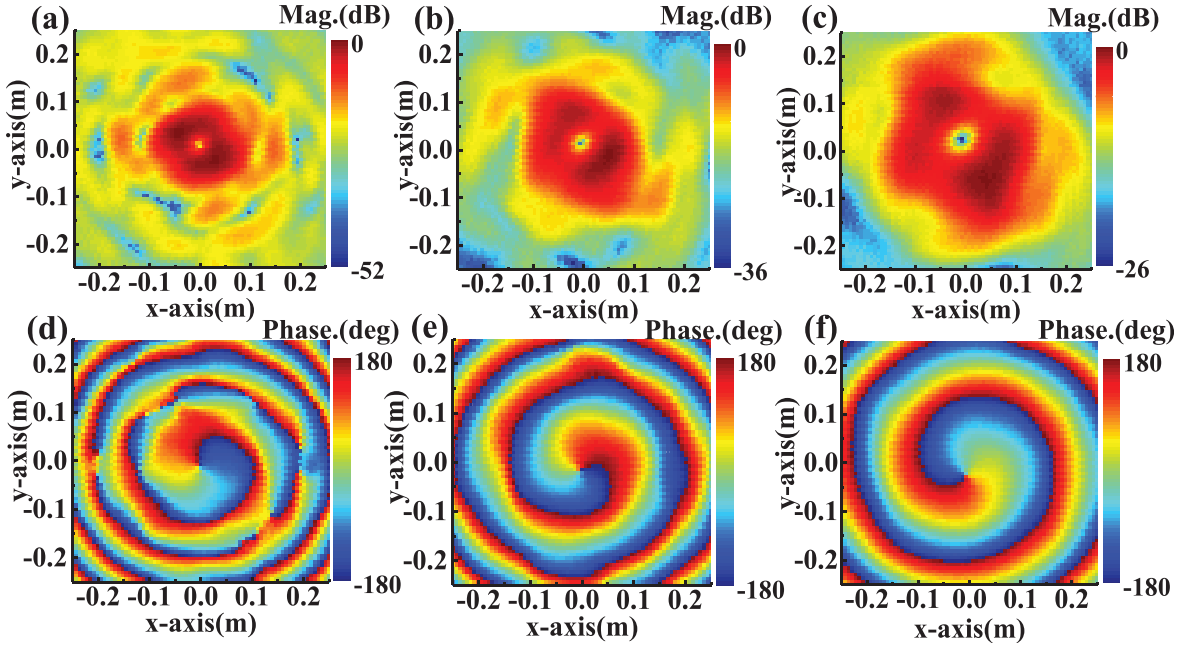

FIG. 10. (a)–(c) Measured amplitude distributions and (d)–(f) phase patterns and on different observation planes located at the cases of 1 m, 1.5 m, and 2 m away from the antenna for Bessel vortex wave at 20 GHz.

distance, which is roughly consistent with the simulation results that are shown in Fig. 7. Meanwhile, the vortex phase pattern behavior can be clearly seen from the measurement results, and the variation of 360° in phase along one circle also conforms to the first-order OAM feature.

In conclusion, this paper discusses the possibility of generating a linearly polarized pseudo-Bessel vortex wave within a large propagation depth of a several hundreds of wavelengths based on an anisotropic holographic impedance metasurface. Compared with other generation methods, the proposed methodology has significant advantages in terms of ultra-low profile, low cost, easy fabrication, and integration. At the same time, it allows for the flexible control of polarization and beam radiation. In addition, the good agreement between the simulated results and the experimental measurements validates our design process, laying a solid foundation for the potential applications of the Bessel vortex beam to imaging, object detection, and identification.

This work was supported in part by the China Postdoctoral Science Foundation under Grant No. 2020M683482, the National

Natural Science Foundation of China under Grant No. 61801366, the National Natural Science Foundation of Shaanxi Province under Grant No. 2020JM-078, and the State Key Laboratory of Millimeter Waves under Grant No. K201933.

DATA AVAILABILITY

The data that support the findings of this study are available from the corresponding author upon reasonable request.

REFERENCES

[1]J. Durnin, J. Opt. Soc. Am. A **4**, 651 (1987).
[2]A. Mazzinghi and A. Freni, IEEE Antennas Wireless Propag. Lett. **16**, 1747 (2017).
[3]Q. Zhang, X. M. Cheng, H. W. Chen, B. He, Z. Y. Ren, Y. Zhang, and J. T. Bai, Appl. Phys. Lett. **111**, 161103 (2017).
[4]M. He, Z. Chen, S. Sun, and J. Pu, Opt. Commun. **294**, 36 (2013).
[5]M. Mazilu, D. J. Stevenson, F. Gunn-Moore, and K. Dholakia, Laser Photonics Rev. **4**, 529 (2010).
[6]L. Allen, M. W. Beijersbergen, R. J. C. Spreeuw, and J. P. Woerdman, Phys. Rev. A **45**, 8185 (1992).
[7]B. Thide, H. Then, J. Sjoholm, K. Palmer, J. Bergman, T. D. Carozzi, Y. N. Istomin, N. H. Ibragimov, and R. Khamitova, Phys. Rev. Lett. **99**, 087701 (2007).
[8]F. Tamburini, E. Mari, A. Sponselli, F. Romanato, B. Thidé, A. Bianchini, L. Palmieri, and C. G. Someda, New J. Phys. **14**, 033001 (2012).
[9]X. Gao, S. Huang, Y. Wei, W. Zhai, W. Xu, S. Yin, J. Zhou, and W. Gu, Appl. Phys. Lett. **105**, 241109 (2014).
[10]F. Tamburini, E. Mari, B. Thideì, C. Barbieri, and F. Romanato, Appl. Phys. Lett. **99**, 204102 (2011).
[11]E. Mari, F. Spinello, M. Oldoni, R. A. Ravanelli, F. Romanato, and G. Parisi, IEEE Antennas Wireless Propag. Lett. **14**, 556 (2015).
[12]J. Ren and K. W. Leung, Appl. Phys. Lett. **112**, 131103–131101 (2018).
[13]S. Yu, L. Li, G. Shi, C. Zhu, and Y. Shi, Appl. Phys. Lett. **108**, 241901 (2016).
[14]S. Yu, L. Li, G. Shi, C. Zhu, X. Zhou, and Y. Shi, Appl. Phys. Lett. **108**, 121903 (2016).
[15]G. Ding, K. Chen, X. Luo, J. Zhao, T. Jiang, and Y. Feng, Phys. Rev. Appl. **11**, 044043 (2019).
[16]L. Ma, C. Chen, L. Zhou, S. Jiang, and H. Zhang, Appl. Phys. Lett. **114**, 081603 (2019).
[17]X. Chen, W. Xue, H. Shi, L. Wang, S. Zhu, and A. Zhang, IEEE Microwave Wireless Compon. Lett. **29**, 560 (2019).
[18]X. Chen, W. Xue, H. Shi, J. Yi, and W. E. I. Sha, IEEE Microwave Wireless Compon. Lett. **30**, 112 (2020).
[19]X. Wei, C. Liu, L. Niu, Z. Zhang, K. Wang, Z. Yang, and J. Liu, Appl. Opt. **54**, 10641–10649 (2015).
[20]N. Kou, S. Yu, and L. Li, Appl. Phys. Express **10**, 016701 (2017).
[21]M. R. Akram, M. Q. Mehmood, T. Tauseef, and A. S. Rana, "Highly efficient generation of Bessel beams with polarization insensitive metasurfaces," Opt. Express **27**, 9467 (2019).
[22]Y. Shen, J. Yang, H. Meng, W. Dou, and S. Hu, Appl. Phys. Lett. **112**, 141901 (2018).
[23]K. Zhang, Y. Yuan, D. Zhang, X. Ding, B. Ratni, S. N. Burokur, M. Lu, K. Tang, and Q. Wu, Opt. Express **26**, 1351 (2018).
[24]L. Yu, X. Li, Z. Qi, H. Zhu, Y. Huang, and Z. Akram, IEEE Antennas Wireless Propag. Lett. **19**, 1226 (2020).
[25]J. Yi, D. Li, R. Feng, B. Ratni, Z. H. Jiang, A. De Lustrac, D. H. Werner, and S. N. Burokur, Appl. Phys. Express **12**, 084501 (2019).
[26]J. Yi, M. Guo, R. Feng, B. Ratni, L. Zhu, D. H. Werner, and S. N. Burokur, Phys. Rev. Appl. **12**, 034060 (2019).
[27]Y. Meng, J. Yi, S. N. Burokur, L. Kang, H. Zhang, and D. H. Werner, Opt. Express **26**, 22019 (2018).
[28]A. Mazzinghi, M. Balma, D. Devona, G. Guarnieri, G. Mauriello, M. Albani, and A. Freni, IEEE Trans. Antennas Propag. **62**, 3911 (2014).
[29]D. Comite, G. Valerio, M. Albani, A. Galli, M. Casaletti, and M. Ettorre, IEEE Trans. Antennas Propag. **65**, 2123 (2017).
[30]B. G. Cai, Y. B. Li, W. X. Jiang, Q. Cheng, and T. J. Cui, Opt. Express **23**, 7593 (2015).
[31]B. H. Fong, J. S. Colburn, J. J. Ottusch, J. L. Visher, and D. F. Sievenpiper, IEEE Trans. Antennas Propag. **58**, 3212 (2010).
[32]X. Meng, J. Wu, Z. Wu, T. Qu, and L. Yang, J. Phys. D: Appl. Phys. **52**, 305002 (2019).
[33]X. Meng, J. Wu, Z. Wu, L. Yang, L. Huang, X. Li, T. Qu, and Z. Wu, Appl. Phys. Lett **114**, 093504 (2019).